# Search for anomalous production of multiple leptons in association with *W* and *Z* bosons at CDF

T. Aaltonen,[21] B. Álvarez González,[9,z] S. Amerio,[40a] D. Amidei,[32] A. Anastassov,[15,x] A. Annovi,[17] J. Antos,[12]
G. Apollinari,[15] J. A. Appel,[15] T. Arisawa,[54] A. Artikov,[13] J. Asaadi,[49] W. Ashmanskas,[15] B. Auerbach,[57] A. Aurisano,[49]
F. Azfar,[39] W. Badgett,[15] T. Bae,[25] A. Barbaro-Galtieri,[26] V. E. Barnes,[44] B. A. Barnett,[23] P. Barria,[42c,42a] P. Bartos,[12]
M. Bauce,[40b,40a] F. Bedeschi,[42a] S. Behari,[23] G. Bellettini,[42b,42a] J. Bellinger,[56] D. Benjamin,[14] A. Beretvas,[15] A. Bhatti,[46]
D. Bisello,[40b,40a] I. Bizjak,[28] K. R. Bland,[5] B. Blumenfeld,[23] A. Bocci,[14] A. Bodek,[45] D. Bortoletto,[44] J. Boudreau,[43]
A. Boveia,[11] L. Brigliadori,[6b,6a] C. Bromberg,[33] E. Brucken,[21] J. Budagov,[13] H. S. Budd,[45] K. Burkett,[15] G. Busetto,[40b,40a]
P. Bussey,[19] A. Buzatu,[31] A. Calamba,[10] C. Calancha,[29] S. Camarda,[4] M. Campanelli,[28] M. Campbell,[32] F. Canelli,[11,15]
B. Carls,[22] D. Carlsmith,[56] R. Carosi,[58a] S. Carrillo,[16,m] S. Carron,[15] B. Casal,[9,l] M. Casarsa,[50a] A. Castro,[6b,6a]
P. Catastini,[20] D. Cauz,[50a] V. Cavaliere,[22] M. Cavalli-Sforza,[4] A. Cerri,[26,g] L. Cerrito,[28,s] Y. C. Chen,[1] M. Chertok,[7]
G. Chiarelli,[58a] G. Chlachidze,[15] F. Chlebana,[15] K. Cho,[25] D. Chokheli,[13] W. H. Chung,[56] Y. S. Chung,[45]
M. A. Ciocci,[42c,42a] A. Clark,[18] C. Clarke,[55] G. Compostella,[40b,40a] M. E. Convery,[15] J. Conway,[7] M. Corbo,[15]
M. Cordelli,[17] C. A. Cox,[7] D. J. Cox,[7] F. Crescioli,[42b,42a] J. Cuevas,[9,z] R. Culbertson,[15] D. Dagenhart,[15] N. d'Ascenzo,[15,w]
M. Datta,[15] P. de Barbaro,[45] M. Dell'Orso,[42b,42a] L. Demortier,[46] M. Deninno,[6a] F. Devoto,[21] M. d'Errico,[40b,40a]
A. Di Canto,[42b,42a] B. Di Ruzza,[15] J. R. Dittmann,[5] M. D'Onofrio,[27] S. Donati,[42b,42a] P. Dong,[15] M. Dorigo,[50a] T. Dorigo,[40a]
K. Ebina,[54] A. Elagin,[49] A. Eppig,[32] R. Erbacher,[7] S. Errede,[22] N. Ershaidat,[15,dd] R. Eusebi,[49] S. Farrington,[39] M. Feindt,[24]
J. P. Fernandez,[29] R. Field,[16] G. Flanagan,[15,u] R. Forrest,[7] M. J. Frank,[5] M. Franklin,[20] J. C. Freeman,[15] H. Frisch,[11]
Y. Funakoshi,[54] I. Furic,[16] M. Gallinaro,[46] J. E. Garcia,[18] A. F. Garfinkel,[44] P. Garosi,[42c,42a] H. Gerberich,[22] E. Gerchtein,[15]
S. Giagu,[47a] V. Giakoumopoulou,[3] P. Giannetti,[42a] K. Gibson,[43] C. M. Ginsburg,[15] N. Giokaris,[3] P. Giromini,[17]
G. Giurgiu,[23] V. Glagolev,[13] D. Glenzinski,[15] M. Gold,[35] D. Goldin,[49] N. Goldschmidt,[16] A. Golossanov,[15] G. Gomez,[9]
G. Gomez-Ceballos,[30] M. Goncharov,[30] O. González,[29] I. Gorelov,[35] A. T. Goshaw,[14] K. Goulianos,[46] S. Grinstein,[4]
C. Grosso-Pilcher,[11] R. C. Group,[53,15] J. Guimaraes da Costa,[20] S. R. Hahn,[15] E. Halkiadakis,[48] A. Hamaguchi,[38]
J. Y. Han,[45] F. Happacher,[17] K. Hara,[51] D. Hare,[48] M. Hare,[52] R. F. Harr,[55] K. Hatakeyama,[5] C. Hays,[39] M. Heck,[24]
J. Heinrich,[41] M. Herndon,[56] S. Hewamanage,[5] A. Hocker,[15] W. Hopkins,[15,h] D. Horn,[24] S. Hou,[1] R. E. Hughes,[36]
M. Hurwitz,[11] U. Husemann,[57] N. Hussain,[31] M. Hussein,[33] J. Huston,[33] G. Introzzi,[42a] M. Iori,[42d,47a] A. Ivanov,[7,q]
E. James,[15] D. Jang,[10] B. Jayatilaka,[14] E. J. Jeon,[25] S. Jindariani,[15] M. Jones,[44] K. K. Joo,[25] S. Y. Jun,[10] T. R. Junk,[15]
T. Kamon,[25,49] P. E. Karchin,[55] A. Kasmi,[5] Y. Kato,[38,p] W. Ketchum,[11] J. Keung,[41] V. Khotilovich,[49] B. Kilminster,[15]
D. H. Kim,[25] H. S. Kim,[25] J. E. Kim,[25] M. J. Kim,[17] S. B. Kim,[25] S. H. Kim,[51] Y. K. Kim,[11] Y. J. Kim,[25] N. Kimura,[54]
M. Kirby,[15] S. Klimenko,[16] K. Knoepfel,[15] K. Kondo,[54,a] D. J. Kong,[25] J. Konigsberg,[16] A. V. Kotwal,[14] M. Kreps,[24]
J. Kroll,[41] D. Krop,[11] M. Kruse,[14] V. Krutelyov,[49,d] T. Kuhr,[24] M. Kurata,[51] S. Kwang,[11] A. T. Laasanen,[44] S. Lami,[42a]
S. Lammel,[15] M. Lancaster,[28] R. L. Lander,[7] K. Lannon,[36,y] A. Lath,[48] G. Latino,[42b,42a] T. LeCompte,[2] E. Lee,[49]
H. S. Lee,[25,11] J. S. Lee,[25] S. W. Lee,[49,bb] S. Leo,[42b,42a] S. Leone,[42a] J. D. Lewis,[15] A. Limosani,[14,t] C.-J. Lin,[26]
M. Lindgren,[15] E. Lipeles,[41] A. Lister,[18] D. O. Litvintsev,[15] C. Liu,[43] H. Liu,[53] Q. Liu,[44] T. Liu,[15] S. Lockwitz,[57]
A. Loginov,[57] D. Lucchesi,[40b,40a] J. Lueck,[24] P. Lujan,[26] P. Lukens,[15] G. Lungu,[46] J. Lys,[26] R. Lysak,[12,f] R. Madrak,[15]
K. Maeshima,[15] P. Maestro,[42c,42a] S. Malik,[46] G. Manca,[27,b] A. Manousakis-Katsikakis,[3] F. Margaroli,[47a] C. Marino,[24]
M. Martínez,[4] P. Mastrandrea,[47a] K. Matera,[22] M. E. Mattson,[55] A. Mazzacane,[15] P. Mazzanti,[59] K. S. McFarland,[45]
P. McIntyre,[49] R. McNulty,[27,k] A. Mehta,[27] P. Mehtala,[21] C. Mesropian,[46] T. Miao,[15] D. Mietlicki,[32] A. Mitra,[1]
H. Miyake,[51] S. Moed,[15] N. Moggi,[6a] M. N. Mondragon,[15,n] C. S. Moon,[25] R. Moore,[15] M. J. Morello,[42d,42a] J. Morlock,[24]
P. Movilla Fernandez,[15] A. Mukherjee,[15] Th. Muller,[24] P. Murat,[15] M. Mussini,[6b,6a] J. Nachtman,[15,o] Y. Nagai,[51]
J. Naganoma,[54] I. Nakano,[37] A. Napier,[52] J. Nett,[49] C. Neu,[53] M. S. Neubauer,[22] J. Nielsen,[26,e] L. Nodulman,[2] S. Y. Noh,[25]
O. Norniella,[22] L. Oakes,[39] S. H. Oh,[14] Y. D. Oh,[25] I. Oksuzian,[53] T. Okusawa,[38] R. Orava,[21] L. Ortolan,[4]
S. Pagan Griso,[40b,40a] C. Pagliarone,[50a] E. Palencia,[9,g] V. Papadimitriou,[15] A. A. Paramonov,[2] J. Patrick,[15]
G. Pauletta,[50a,50b] M. Paulini,[10] C. Paus,[30] D. E. Pellett,[7] A. Penzo,[60a] T. J. Phillips,[14] G. Piacentino,[42a] E. Pianori,[41]
J. Pilot,[36] K. Pitts,[22] C. Plager,[8] L. Pondrom,[56] S. Poprocki,[15,h] K. Potamianos,[44] F. Prokoshin,[13,cc] A. Pranko,[26]
F. Ptohos,[17,i] G. Punzi,[42b,42a] A. Rahaman,[43] V. Ramakrishnan,[56] N. Ranjan,[44] I. Redondo,[29] P. Renton,[39] M. Rescigno,[61a]
T. Riddick,[28] F. Rimondi,[6b,6a] L. Ristori,[42a,15] A. Robson,[19] T. Rodrigo,[9] T. Rodriguez,[41] E. Rogers,[22] S. Rolli,[52,j]
R. Roser,[15] F. Ruffini,[42c,42a] A. Ruiz,[9] J. Russ,[10] V. Rusu,[15] A. Safonov,[49] W. K. Sakumoto,[45] Y. Sakurai,[54] L. Santi,[50b,50a]
K. Sato,[51] V. Saveliev,[15,w] A. Savoy-Navarro,[15,aa] P. Schlabach,[15] A. Schmidt,[24] E. E. Schmidt,[15] T. Schwarz,[15]
L. Scodellaro,[9] A. Scribano,[42c,42a] F. Scuri,[42a] S. Seidel,[35] Y. Seiya,[38] A. Semenov,[13] F. Sforza,[42c,42a] S. Z. Shalhout,[7]
T. Shears,[27] P. F. Shepard,[43] M. Shimojima,[51,v] M. Shochet,[11] I. Shreyber-Tecker,[34] A. Simonenko,[13] P. Sinervo,[31]

K. Sliwa,[52] J. R. Smith,[7] F. D. Snider,[15] A. Soha,[15] V. Sorin,[4] H. Song,[43] P. Squillacioti,[42c,42a] M. Stancari,[15] R. St. Denis,[19] B. Stelzer,[31] O. Stelzer-Chilton,[31] D. Stentz,[15,x] J. Strologas,[35] G. L. Strycker,[32] Y. Sudo,[51] A. Sukhanov,[15] I. Suslov,[13] K. Takemasa,[51] Y. Takeuchi,[51] J. Tang,[11] M. Tecchio,[32] P. K. Teng,[1] J. Thom,[15,h] J. Thome,[10] G. A. Thompson,[22] E. Thomson,[41] D. Toback,[49] S. Tokar,[12] K. Tollefson,[33] T. Tomura,[51] D. Tonelli,[15] S. Torre,[17] D. Torretta,[15] P. Totaro,[40a] M. Trovato,[42d,42a] F. Ukegawa,[51] S. Uozumi,[25] A. Varganov,[32] F. Vázquez,[16,n] G. Velev,[15] C. Vellidis,[15] M. Vidal,[44] I. Vila,[9] R. Vilar,[9] J. Vizán,[9] M. Vogel,[35] G. Volpi,[17] P. Wagner,[41] R. L. Wagner,[15] T. Wakisaka,[38] R. Wallny,[8] S. M. Wang,[1] A. Warburton,[31] D. Waters,[28] W. C. Wester III,[15] D. Whiteson,[41,c] A. B. Wicklund,[2] E. Wicklund,[15] S. Wilbur,[11] F. Wick,[24] H. H. Williams,[41] J. S. Wilson,[36] P. Wilson,[15] B. L. Winer,[36] P. Wittich,[15,h] S. Wolbers,[15] H. Wolfe,[36] T. Wright,[32] X. Wu,[18] Z. Wu,[5] K. Yamamoto,[38] D. Yamato,[38] T. Yang,[15] U. K. Yang,[11,r] Y. C. Yang,[25] W.-M. Yao,[26] G. P. Yeh,[15] K. Yi,[15,o] J. Yoh,[15] K. Yorita,[54] T. Yoshida,[38,m] G. B. Yu,[14] I. Yu,[25] S. S. Yu,[15] J. C. Yun,[15] A. Zanetti,[50a] Y. Zeng,[14] and S. Zucchelli[6b,6a]

(CDF Collaboration)

[1]*Institute of Physics, Academia Sinica, Taipei, Taiwan 11529, Republic of China*
[2]*Argonne National Laboratory, Argonne, Illinois 60439, USA*
[3]*University of Athens, 157 71 Athens, Greece*
[4]*Institut de Fisica d'Altes Energies, ICREA, Universitat Autonoma de Barcelona, E-08193, Bellaterra (Barcelona), Spain*
[5]*Baylor University, Waco, Texas 76798, USA*
[6a]*Istituto Nazionale di Fisica Nucleare Bologna, I-40127 Bologna, Italy*
[6b]*University of Bologna, I-40127 Bologna, Italy*
[7]*University of California, Davis, Davis, California 95616, USA*
[8]*University of California, Los Angeles, Los Angeles, California 90024, USA*
[9]*Instituto de Fisica de Cantabria, CSIC-University of Cantabria, 39005 Santander, Spain*
[10]*Carnegie Mellon University, Pittsburgh, Pennsylvania 15213, USA*
[11]*Enrico Fermi Institute, University of Chicago, Chicago, Illinois 60637, USA*
[12]*Comenius University, 842 48 Bratislava, Slovakia; Institute of Experimental Physics, 040 01 Kosice, Slovakia*
[13]*Joint Institute for Nuclear Research, RU-141980 Dubna, Russia*
[14]*Duke University, Durham, North Carolina 27708, USA*
[15]*Fermi National Accelerator Laboratory, Batavia, Illinois 60510, USA*
[16]*University of Florida, Gainesville, Florida 32611, USA*
[17]*Laboratori Nazionali di Frascati, Istituto Nazionale di Fisica Nucleare, I-00044 Frascati, Italy*
[18]*University of Geneva, CH-1211 Geneva 4, Switzerland*
[19]*Glasgow University, Glasgow G12 8QQ, United Kingdom*
[20]*Harvard University, Cambridge, Massachusetts 02138, USA*
[21]*Division of High Energy Physics, Department of Physics, University of Helsinki and Helsinki Institute of Physics, FIN-00014, Helsinki, Finland*
[22]*University of Illinois, Urbana, Illinois 61801, USA*
[23]*The Johns Hopkins University, Baltimore, Maryland 21218, USA*
[24]*Institut für Experimentelle Kernphysik, Karlsruhe Institute of Technology, D-76131 Karlsruhe, Germany*
[25]*Center for High Energy Physics: Kyungpook National University, Daegu 702-701, Korea; Seoul National University, Seoul 151-742, Korea; Sungkyunkwan University, Suwon 440-746, Korea; Korea Institute of Science and Technology Information, Daejeon 305-806, Korea; Chonnam National University, Gwangju 500-757, Korea; Chonbuk National University, Jeonju 561-756, Korea*
[26]*Ernest Orlando Lawrence Berkeley National Laboratory, Berkeley, California 94720, USA*
[27]*University of Liverpool, Liverpool L69 7ZE, United Kingdom*
[28]*University College London, London WC1E 6BT, United Kingdom*
[29]*Centro de Investigaciones Energeticas Medioambientales y Tecnologicas, E-28040 Madrid, Spain*
[30]*Massachusetts Institute of Technology, Cambridge, Massachusetts 02139, USA*
[31]*Institute of Particle Physics: McGill University, Montréal, Québec, Canada H3A 2T8; Simon Fraser University, Burnaby, British Columbia, Canada V5A 1S6; University of Toronto, Toronto, Ontario, Canada M5S 1A7; and TRIUMF, Vancouver, British Columbia, Canada V6T 2A3*
[32]*University of Michigan, Ann Arbor, Michigan 48109, USA*
[33]*Michigan State University, East Lansing, Michigan 48824, USA*
[34]*Institution for Theoretical and Experimental Physics, ITEP, Moscow 117259, Russia*
[35]*University of New Mexico, Albuquerque, New Mexico 87131, USA*
[36]*The Ohio State University, Columbus, Ohio 43210, USA*
[37]*Okayama University, Okayama 700-8530, Japan*
[38]*Osaka City University, Osaka 588, Japan*

[39]*University of Oxford, Oxford OX1 3RH, United Kingdom*
[40a]*Istituto Nazionale di Fisica Nucleare, Sezione di Padova-Trento, I-35131 Padova, Italy*
[40b]*University of Padova, I-35131 Padova, Italy*
[41]*University of Pennsylvania, Philadelphia, Pennsylvania 19104, USA*
[42a]*Istituto Nazionale di Fisica Nucleare Pisa, I-56127 Pisa, Italy*
[42b]*University of Pisa, I-56127 Pisa, Italy*
[42c]*University of Siena, I-56127 Pisa, Italy*
[42d]*Scuola Normale Superiore, I-56127 Pisa, Italy*
[43]*University of Pittsburgh, Pittsburgh, Pennsylvania 15260, USA*
[44]*Purdue University, West Lafayette, Indiana 47907, USA*
[45]*University of Rochester, Rochester, New York 14627, USA*
[46]*The Rockefeller University, New York, New York 10065, USA*
[47a]*Istituto Nazionale di Fisica Nucleare, Sezione di Roma 1, I-00185 Roma, Italy*
[47b]*Sapienza Università di Roma, I-00185 Roma, Italy*
[48]*Rutgers University, Piscataway, New Jersey 08855, USA*
[49]*Texas A&M University, College Station, Texas 77843, USA*
[50a]*Istituto Nazionale di Fisica Nucleare Trieste/Udine, I-34100 Trieste, I-33100 Udine, Italy*
[50b]*University of Udine, I-33100 Udine, Italy*
[51]*University of Tsukuba, Tsukuba, Ibaraki 305, Japan*
[52]*Tufts University, Medford, Massachusetts 02155, USA*
[53]*University of Virginia, Charlottesville, Virginia 22906, USA*
[54]*Waseda University, Tokyo 169, Japan*
[55]*Wayne State University, Detroit, Michigan 48201, USA*
[56]*University of Wisconsin, Madison, Wisconsin 53706, USA*
[57]*Yale University, New Haven, Connecticut 06520, USA*
[58a]*Istituto Nazionale di Fisica Nucleare Pisa, I-56127 Pisa, Italy*
[58b]*University of Pisa, I-56127 Pisa, Italy*
[58c]*University of Siena, I-56127 Pisa, Italy*
[58d]*Scuola Normale Superiore, I-56127 Pisa, Italy*

[a]Deceased.
[b]Visitor from Istituto Nazionale di Fisica Nucleare, Sezione di Cagliari, 09042 Monserrato (Cagliari), Italy.
[c]Visitor from University of California Irvine, Irvine, CA 92697, USA.
[d]Visitor from University of California Santa Barbara, Santa Barbara, CA 93106, USA.
[e]Visitor from University of California Santa Cruz, Santa Cruz, CA 95064, USA.
[f]Visitor from Institute of Physics, Academy of Sciences of the Czech Republic, Czech Republic.
[g]Visitor from CERN, CH-1211 Geneva, Switzerland.
[h]Visitor from Cornell University, Ithaca, NY 14853, USA.
[i]Visitor from University of Cyprus, Nicosia CY-1678, Cyprus.
[j]Visitor from Office of Science, U.S. Department of Energy, Washington, DC 20585, USA.
[k]Visitor from University College Dublin, Dublin 4, Ireland.
[l]Visitor from ETH, 8092 Zurich, Switzerland.
[m]Visitor from University of Fukui, Fukui City, Fukui Prefecture, Japan 910-0017.
[n]Visitor from Universidad Iberoamericana, Mexico D.F., Mexico.
[o]Visitor from University of Iowa, Iowa City, IA 52242, USA.
[p]Visitor from Kinki University, Higashi-Osaka City, Japan 577-8502.
[q]Visitor from Kansas State University, Manhattan, KS 66506, USA.
[r]Visitor from University of Manchester, Manchester M13 9PL, United Kingdom.
[s]Visitor from Queen Mary, University of London, London, E1 4NS, United Kingdom.
[t]Visitor from University of Melbourne, Victoria 3010, Australia.
[u]Visitor from Muons, Inc., Batavia, IL 60510, USA.
[v]Visitor from Nagasaki Institute of Applied Science, Nagasaki, Japan.
[w]Visitor from National Research Nuclear University, Moscow, Russia.
[x]Visitor from Northwestern University, Evanston, IL 60208, USA.
[y]Visitor from University of Notre Dame, Notre Dame, IN 46556, USA.
[z]Visitor from Universidad de Oviedo, E-33007 Oviedo, Spain.
[aa]Visitor from CNRS-IN2P3, Paris, F-75252 France.
[bb]Visitor from Texas Tech University, Lubbock, TX 79609, USA.
[cc]Visitor from Universidad Tecnica Federico Santa Maria, 110v Valparaiso, Chile.
[dd]Visitor from Yarmouk University, Irbid 211-63, Jordan.

[59]*Istituto Nazionale di Fisica Nucleare Bologna, University of Bologna, I-40127 Bologna, Italy*
[60a]*Istituto Nazionale di Fisica Nucleare Trieste/Udine, I-34100 Trieste*
[60b]*University of Udine, I-33100 Udine, Italy*
[61a]*Istituto Nazionale di Fisica Nucleare, Sezione di Roma 1, I-00185 Roma, Italy*
[61b]*Sapienza Università di Roma, I-00185 Roma, Italy*

This paper presents a search for anomalous production of multiple low-energy leptons in association with a $W$ or $Z$ boson using events collected at the CDF experiment corresponding to 5.1 fb$^{-1}$ of integrated luminosity. This search is sensitive to a wide range of topologies with low-momentum leptons, including those with the leptons near one another. The observed rates of production of additional electrons and muons are compared with the standard model predictions. No indications of phenomena beyond the standard model are found. A 95% confidence level limit is presented on the production cross section for a benchmark model of supersymmetric hidden-valley Higgs production. Particle identification efficiencies are also provided to enable the calculation of limits on additional models.

## I. INTRODUCTION

The signature of multiple leptons is common in many models of physics beyond the standard model (SM) with light mass scales and couplings to the electroweak sector, such as the next-to-minimal supersymmetric model [1], little Higgs models [2], and $R$-parity violating minimal supersymmetric standard models (MSSM) [3]. Some of these new physics scenarios propose explanations for the nature of dark matter [4] as well as the existence of other, yet-undiscovered particles in long decay chains. In addition to predicting large numbers of leptons, these models also often predict that clusters of leptons are produced spatially close to each other. These clusters are often referred to in the literature as ''lepton jets'' [5]. Because of the unique characteristics of these models, they could have evaded previous searches for an excess of leptons, such as diboson searches [6] and SUSY-inspired multi-lepton searches [7]. The high multiplicity of leptons can lead to low lepton momenta, well below the usual cutoff of 10–20 GeV. Additionally, collimated lepton jets will fail the standard requirement that leptons be isolated in the detector. As an example, Fig. 1 shows a typical decay chain in a model in which the Higgs decays to a light hidden sector resulting in events with a high multiplicity of leptons [8].

This paper presents a signature-based search for anomalous production of multiple electrons and/or muons in association with $W$ and $Z$ bosons. Previous searches for lepton jets at the Tevatron [9] and at the LHC [10] have focused on searching for clusters of leptons with specific requirements on the size of the clusters. These searches have resulted in no evidence for lepton jets. We have performed a more general search, sensitive to a wide range of scenarios that predict multiple electrons and muons. Note that hadronic decays of tau leptons are not included in this search due to the additional difficulty in identifying them in nonisolated topologies.

The data used here correspond to 5.1 fb$^{-1}$ of integrated luminosity at a center-of-mass energy of $\sqrt{s} = 1.96$ TeV collected using the CDF detector at Fermilab between December 2004 and January 2010. Within the events containing leptonically decaying $W$ and $Z$ bosons, we search for additional ''soft'' leptons with no isolation requirements and with momentum greater than 3 GeV for muons and 2 GeV for electrons [11].
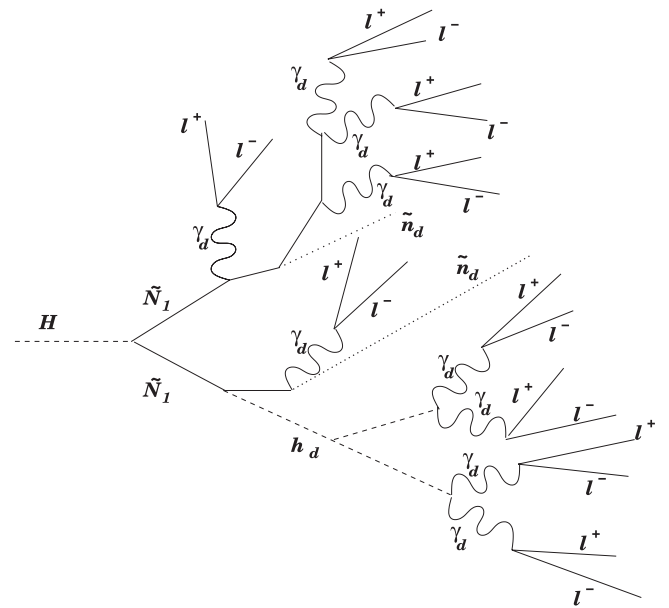


FIG. 1. An example of multiple low-$p_T$, nonisolated lepton production. A Higgs decays to a pair of lightest supersymmetric neutralinos ($\tilde{N}_1$) which then cascade through a dark sector to a lightest dark sector particle ($\tilde{n}_d$) and a number of dark photons ($\gamma_d$). The dark photons then decay back into the SM in the form of leptons ($l^\pm$). This model is adapted from Ref. [8]. Note that this diagram shows only the decay of the Higgs, while this analysis as a whole would be sensitive to the associated production of a Higgs with a $W$ or $Z$ boson.

## II. ANALYSIS STRATEGY

The analysis strategy and the structure of this paper are as follows. The baseline data sets for this analysis consist of leptonically decaying $W$ and $Z$ boson events selected with high transverse momentum [12] ($p_T$) leptons [13]. The kinematic distributions are used to validate the $W$ and $Z$ boson selections. The selection of these events is described in Sec. IV.

After the $W$ or $Z$ boson reconstruction, additional low-$p_T$ electrons and muons are identified in the events with no isolation requirements. Purely data-driven techniques are used to develop the soft lepton identification algorithms. The selection of soft leptons is more fully described in Sec. V.

The numbers of additional electrons and muons are counted in the inclusive $W$ and $Z$ data sets, where the SM predicts few events with multiple leptons. The observed event count is compared to the SM expectations in bins of additional lepton multiplicity. These results are described in Sec. VII.

## III. THE CDF-II DETECTOR

The CDF-II detector is a cylindrically symmetric spectrometer designed to study $p\bar{p}$ collisions at the Fermilab Tevatron. The detector has been extensively described in detail elsewhere in the literature [14]. Here the detector subsystems relevant for this analysis are described.

Tracking systems are used to measure the momenta of charged particles, to reconstruct primary and secondary vertices, and to trigger on and identify leptons with large transverse momentum. Silicon strip detectors [15] and the central outer tracker (COT) [16] are contained in a superconducting solenoid that generates a magnetic field of 1.4 T. The silicon strip system provides up to eight measurements in the $r$-$\phi$ and $r$-$z$ views and helps to reconstruct tracks in the region $|\eta| < 2$ [12]. The COT is an open-cell drift chamber that makes up to 96 measurements along the track of each charged particle in the region $|\eta| < 1$. Sense wires are arranged in eight alternating axial and $\pm 2°$ stereo superlayers. The resolution in $p_T$, $\sigma_{p_T}/p_T$, is $\approx 0.0015 p_T(\text{GeV})$ for tracks with only COT measurements, and $\approx 0.0007 p_T(\text{GeV})$ for tracks with both silicon and COT measurements.

Calorimeters are segmented with towers arranged in a projective geometry. Each tower consists of an electromagnetic and a hadronic compartment [17–19]. The central electromagnetic calorimeter (CEM) and central hadronic calorimeter cover the central region ($|\eta| < 1.1$), while the plug electromagnetic calorimeter (PEM) and plug hadronic calorimeter cover the "end plug" region ($1.1 < |\eta| < 3.6$). In this analysis, a high-$E_T$ electron is required to be identified in the central region, where the CEM has a segmentation of $15°$ in $\phi$ and $\approx 0.1$ in $\eta$ [14], and an $E_T$ resolution of $\sigma(E_T)/E_T \approx 13.5\%/\sqrt{E_T(\text{GeV})} \oplus 2\%$ [17].

Two additional systems in the central region with finer spatial resolution are used for electron identification. The central strip system (CES) uses a multiwire proportional chamber to make profile measurements of electromagnetic showers at a depth of six radiation lengths (approximately shower maximum) [17]. The central preshower detector (CPR) is located just outside the solenoid coil on the front face of the CEM. In 2004 the CPR was upgraded from the run I configuration of wire proportional chambers to a fast scintillator system [19]. This analysis only uses data collected after the CPR upgrade.

Muons are identified using the central muon systems [20]: CMU and CMP for the pseudorapidity region of $|\eta| < 0.6$, and CMX for the pseudorapidity region of $0.6 < |\eta| < 1.0$. The CMU system uses four layers of planar drift chambers to detect muons with $p_T > 1.4$ GeV. The CMP system consists of an additional four layers of planar drift chambers located behind 0.6 m of steel outside the magnetic return yoke, and detects muons with $p_T > 2.2$ GeV. The CMX system detects muons with $p_T > 1.4$ GeV with four to eight layers of drift chambers, depending on the direction of the muon.

The luminosity is measured using two sets of gas Cerenkov counters [21], located in the region $3.7 < |\eta| < 4.7$. The total uncertainty on the luminosity is estimated to be 5.9%, where 4.4% comes from the acceptance and operation of the luminosity monitor and 4.0% from the calculation of the inelastic $p\bar{p}$ cross section [22].

A three-level online event selection (trigger) system [23] selects events to be recorded for further analysis. The first two trigger levels consist of dedicated fast digital electronics analyzing a subset of the complete detector information. The third level, applied to the full set of detector information from those events passing the first two levels, consists of a farm of computers that reconstruct the data and apply selection criteria consistent with the subsequent offline event processing.

## IV. W AND Z BOSON SAMPLE SELECTION

Events for this analysis are selected with three different triggers [23]. Approximately half the events are selected with a trigger requiring a high-$p_T$ central electron in the CEM ($E_T > 18$ GeV, $|\eta| < 1.0$). In addition, two muon triggers, one requiring hits in both the CMP and CMU and the other requiring hits in the CMX, collect events with central muons ($p_T > 18$ GeV, $|\eta| < 1.0$).

Further selection criteria are imposed on triggered events offline. Electron (muon) candidates are required to have $E_T > 20$ GeV ($p_T > 20$ GeV). They must fulfill several other identification criteria designed to select pure samples of high-$p_T$ electrons (muons) [13], including an isolation requirement that the energy within a cone of $\Delta R = \sqrt{\Delta \phi^2 + \Delta \eta^2} < 0.4$ around the lepton direction is less than 10% of the $E_T$ ($p_T$) of the electron (muon).

In order to reduce the electron background from photon conversions, the electron(s) from the $W$ or $Z$ boson decay are required to pass a conversion filter. Electron candidates with an oppositely charged partner track consistent with having originated from a photon conversion are removed [24]. However, the electron candidate is kept if its partner conversion track also has another partner track, since the three tracks are assumed to originate from an electron which radiates a photon which subsequently converts.

In order to reduce the background from mesons decaying to muons within the tracking chamber, the muon(s) from the $W$ or $Z$ boson decay must pass a decay-in-flight removal algorithm. The decay-in-flight algorithm requires the $\chi^2$ per degree of freedom of the fitted track to be less than 3 and requires that the impact parameter of the track be less than 0.02 cm. Additionally, for tracks with $p_T >$ 300 GeV, it requires $N_{\text{transitions}} > 30$, where $N_{\text{transitions}}$ is the number of times the pattern of track hits crosses the fitted track [25]. Muons consistent with cosmic rays are vetoed [26].

To select $W$ boson events we require $\not{E}_T > 25$ GeV and that the highest-energy lepton and the $\not{E}_T$ have $m_T >$ 20 GeV [12]. In order to remove events where the $\not{E}_T$ arises from a mismeasured lepton, the difference in $\phi$ between the highest-energy lepton and the $\vec{\not{E}}_T$ is required to be greater than 0.5 radians. The $Z$ boson selection requires two oppositely charged, same-flavor leptons. One of these leptons is required to pass the above high-$p_T$ lepton identification selections, while the other is required only to pass a less stringent "loose" selection. For muons, the loose selection allows for muons with $p_T \geq$ 10 GeV that have hits in either the CMP, CMU, or CMX systems. For electrons, the loose selection accepts electrons with $E_T \geq 12$ GeV and has relaxed identification requirements with respect to the centroid shape in the CES and $E/p$, the ratio of calorimeter energy to track momentum [27]. Finally, the invariant mass of the lepton pair is required to be within the range of 76 GeV $\leq$ $m(l, l) \leq 106$ GeV, consistent with the mass of the $Z$ boson.

The distributions of $m_T$ in $W$ boson events and the dilepton invariant mass in $Z$ boson events are shown in Fig. 2 for both electron- and muon-triggered events. In total, 4 722 370 $W$ boson events and 342 291 $Z$ boson events are obtained from 5.1 fb$^{-1}$ of data. Good agreement with predictions is observed across most of the distributions. In the $W$ $m_T$ distributions, a disagreement occurs at low mass, where the distribution shifts from being QCD dominated to electroweak dominated, and is accounted for by the QCD normalization systematic uncertainty (as described in Sec. VI A). In the $Z$ selection, a similar mass disagreement is due to the fact that the Monte Carlo (MC) simulation does not include Drell-Yan events with a $Z/\gamma^*$ invariant mass below 8 GeV. It is eliminated with the requirement that the dilepton mass be within the $Z$ peak.
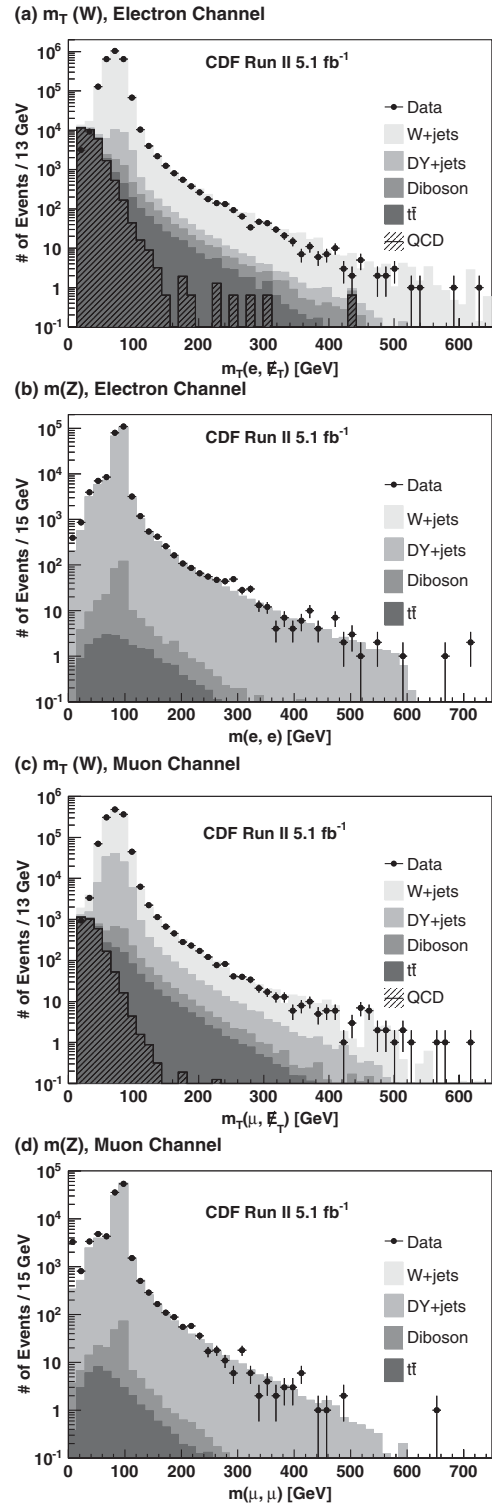


FIG. 2. (a) The transverse mass ($m_T$) of the highest-$p_T$ lepton and the $\not{E}_T$ in the electron-triggered $W$ boson sample. (b) The dilepton invariant mass in the electron-triggered $Z$ boson sample. (c) The $m_T$ of the highest-$p_T$ lepton and the $\not{E}_T$ in the muon-triggered $W$ boson sample. (d) The dilepton invariant mass in the muon-triggered $Z$ boson sample. The estimation of the QCD contribution to these distributions is described in Sec. VI A. The points represent the observed data, and the filled histograms are the SM estimates.

## V. SOFT LEPTON IDENTIFICATION

The identification of low-$p_T$, or "soft," leptons is a main focus of this analysis. Likelihood-based methods are used to identify soft electrons and muons. The identification algorithms are described here, along with the methods used to validate them and evaluate their systematic uncertainties.

### A. Soft electrons

Soft electrons are identified using a likelihood method trained on a signal sample from photon conversions and a background sample from other tracks with electron sources removed.

#### *1. Identification algorithm and candidate selections*

A preselection is applied to all soft electron candidates requiring good track quality as well as track extrapolation to the CES, CPR, and calorimeter. Only tracks with $|\eta| < 1$ are considered for the soft electron identification.

After this preselection, a likelihood-based calculator is used to identify electrons. The likelihood calculator uses seven discriminating variables: the energy loss as the track traverses the tracking chamber, the electromagnetic and hadronic calorimeter energies, the energies deposited in the preradiator and the showermax detector, and the two-dimensional distance $(\Delta x, \Delta z)$ between the extrapolated position of the track and the shower in the CES. The calorimeter variables are calculated using a narrow, two-tower-wide section of the calorimeter.

Some of the variables used in the soft electron identification are modeled very badly in the MC, and so the likelihood is trained on data without resorting to the simulation. For each of the above variables $x_i$, a fit is performed to the ratio of the distribution in the electron sample and the distribution in the nonelectron background ("fake") sample. For each candidate, the values of each of these fit functions are multiplied together to get the final likelihood ($\mathcal{L}_{\text{electron}}$):

$$Q = \prod_i \frac{P(x_i|\text{real})}{P(x_i|\text{fake})}, \qquad \mathcal{L}_{\text{electron}} = \frac{Q}{1+Q}.$$

The distribution of the likelihood in the real and fake samples is shown in Fig. 3. A candidate is identified as an electron if it passes the requirement $\mathcal{L}_{\text{electron}} > 0.99$.

#### *2. Training samples and efficiency and misidentification rate measurements*

Photon conversions are used as a pure sample of electrons to train the likelihood function. In events selected using an 8 GeV electron trigger, pairs of tracks are found that correspond to a photon converting into $e^+e^-$ [24]. In order to avoid any bias from the trigger, the lower-momentum track of the conversion pair is used to train the likelihood.

Events from the 18 GeV muon trigger are used to select a sample of nonelectron tracks with which to train the likelihood function. All tracks in the events that, along with another track, form a possible photon conversion are removed from the training sample. To reduce the bias from using a muon-triggered sample, any track that is within $\Delta R < 0.7$ of an identified muon is also ignored. In addition, to reduce the contamination from real electrons, any event that contains an identified heavy quark decay or an identified high-$p_T$ electron is ignored.

The efficiency and fake rate are calculated in these training samples as functions of $p_T$, $\eta$, and track isolation. The same sample used for training is also used to measure the efficiency, due to the larger backgrounds present in other independent samples. The separation in identification rate between electrons and nonelectrons after the likelihood selection is shown in Fig. 3 (right panel). The efficiency in terms of $p_T$ and $\eta$, after the track and CES shower have been identified, is shown in Table I.
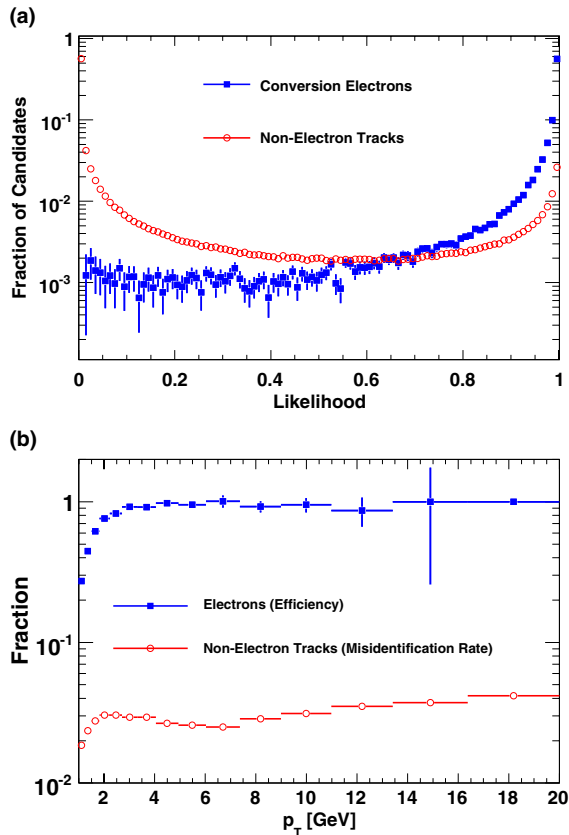
FIG. 3 (color online). (a) The likelihood distributions for electrons (closed squares) and nonelectrons (open circles) after all preselection criteria. Only those candidates with a likelihood >0.99 are identified as electrons. (b) The efficiency as a function of $p_T$ for the identification of electrons (closed squares) and tracks misidentified as electrons (open circles) after the likelihood selection.

TABLE I. Efficiency to identify soft ($2\text{ GeV} < p_T < 20\text{ GeV}$) electrons as a function of candidates $p_T$ and $\eta$.

| $p_T$ range (GeV) | [2, 2.5] | [2.5, 3] | [3, 6] | [6, 12] | [12, 20] |
|---|---|---|---|---|---|
| $0 < \lvert\eta\rvert < 0.2$ | 0.90 | 0.99 | 0.99 | 0.90 | 0.99 |
| $0.2 < \lvert\eta\rvert < 0.6$ | 0.94 | 0.99 | 0.99 | 0.99 | 0.99 |
| $0.6 < \lvert\eta\rvert < 1$ | 0.95 | 0.99 | 0.99 | 0.99 | 0.99 |

This identification rate is applied as a weight to each candidate track in the MC to find the predicted number of identified electrons.

### 3. Validation and systematic uncertainty determination

The efficiency and fake rate parametrizations are checked on a data set triggered on jets having $E_T > 50\text{ GeV}$. The parametrizations use the $p_T$, $\eta$ and isolation of candidates in order to account for any kinematic differences between the training sample and the validation sample. First, the same electron removal that was used for the fake training sample (Sec. VA 2) is applied to the tracks in the jet sample. The likelihood distribution of all candidate tracks in the jet sample is then fit to templates from the real and fake likelihood training samples to obtain the fraction of real and fake electrons in the jet sample. The jet sample is found to consist of 2.5% real electrons, mostly coming from photon conversions from which only one electron was reconstructed. The predicted identification rate is then checked for agreement with the measured identification rate.

The disagreement between the calculated and observed identification rates is measured to be 1.6%. However, we observe larger disagreement in the shapes of the calculated and observed distributions in $p_T$ and $\eta$. We assign a systematic uncertainty of 15%, which is sufficient to cover the observed disagreement [24]. This systematic uncertainty is applied separately to the electron identification and misidentification rates.

### B. Soft muons

Soft muons are identified using a method similar to that described in Ref. [28]. The inputs to the algorithm are derived from a sample of muons arising from $J/\psi$ decays in a muon calibration data set.

#### 1. Identification algorithm and candidate selections

The soft muon identification algorithm relies on matching tracks identified in the COT to track segments reconstructed in the muon chambers (muon stubs). Matching is done in the extrapolated position along the muon chamber drift direction ($x$), the longitudinal coordinate along the chamber wires ($z$) when available, and the difference in slope between the extrapolated COT track and the reconstructed muon chamber track segment ($\phi_L$). Tracks are paired with muon chamber track segments based on the
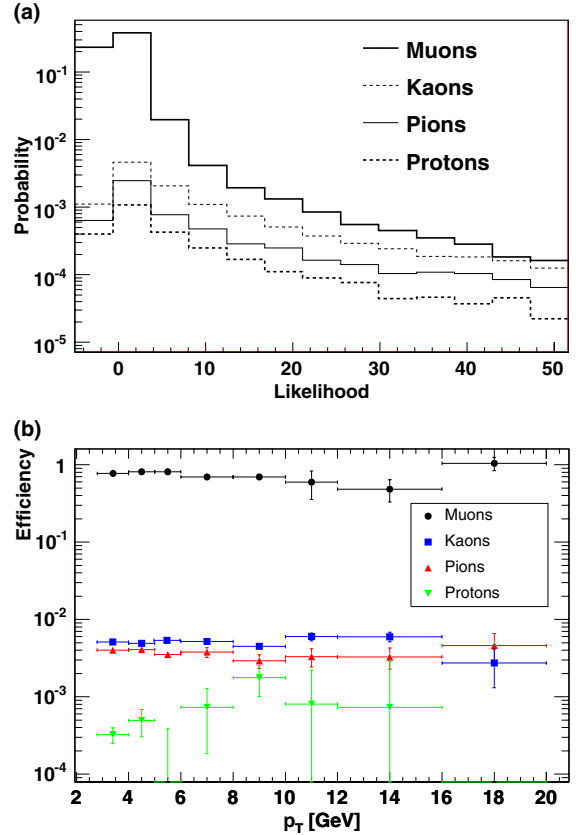


FIG. 4 (color online).   (a) The distribution of soft muon scaled $\chi^2$, $\mathcal{Q}_{\text{muon}}$, for muons, pions, kaons, and protons after all preselection selections. Only those candidates with $\lvert\mathcal{Q}_{\text{muon}}\rvert < 3.5$ are identified as muons. (b) The muon identification rate (circles) and misidentification rates for pions (triangles), kaons (squares), and protons (triangles) after the scaled $\chi^2$ selection.

best match in $x$ for those track segments within 50 cm of an extrapolated COT track.

Soft muon candidates are required to extrapolate to within the physical boundaries of a muon chamber, have good track quality, have at least one hit in the silicon strip detectors, $\lvert d_0\rvert < 0.3$ cm where $d_0$ is the impact parameter with respect to the beam line, and $z_0 < 60$ cm where $z_0$ is the $z$ position of the track at the interaction point.

A $\chi^2$ is built from the track-to-stub matching variables $x_i$ described above ($dx$, $dz$, and $d\phi_L$). This $\chi^2$ is normalized to have mean 0 and variance 1 for real muons, independent of the number $n$ of track-stub matching variables $x_i$ used:

$$\chi^2 = \sum_i \frac{(x_i - \mu_i)^2}{\sigma_i^2}, \qquad \mathcal{Q}_{\text{muon}} = \frac{\chi^2 - n}{\sigma(\chi^2)},$$

where $\mu_i$ and $\sigma_i^2$ are the expected mean and variance of the distribution of $x_i$, and $\sigma(\chi^2)$ is the expected standard deviation of $\chi^2$.

In the final selection, we require that all identified soft muons must have a track segment in each muon chamber to

TABLE II. Efficiency to identify soft muons as a function of candidate $p_T$ and $\eta$.

| $p_T$ range (GeV) | [3, 4] | [4, 5] | [5, 6] | [6, 8] | [8, 10] | [10, 12] | [12, 16] | [16, 20] |
|---|---|---|---|---|---|---|---|---|
| $-1.5 < \eta < -0.7$ | 0.739 | 0.626 | 0.567 | 0.419 | 0.342 | 0.127 | 0.237 | 0.174 |
| $-0.7 < \eta < -0.55$ | 0.593 | 0.556 | 0.581 | 0.480 | 0.438 | 0.299 | 0.356 | 0.344 |
| $-0.55 < \eta < -0.45$ | 0.749 | 0.788 | 0.883 | 0.751 | 0.783 | 0.608 | 0.644 | 0.659 |
| $-0.45 < \eta < -0.15$ | 0.816 | 0.901 | 0.898 | 0.782 | 0.821 | 0.701 | 0.570 | 0.659 |
| $-0.15 < \eta < 0.15$ | 0.777 | 0.796 | 0.784 | 0.667 | 0.657 | 0.525 | 0.424 | 0.616 |
| $0.15 < \eta < 0.45$ | 0.832 | 0.918 | 0.913 | 0.799 | 0.815 | 0.698 | 0.568 | 0.659 |
| $0.45 < \eta < 0.55$ | 0.768 | 0.782 | 0.840 | 0.741 | 0.582 | 0.758 | 0.529 | 0.659 |
| $0.55 < \eta < 0.7$ | 0.625 | 0.573 | 0.556 | 0.461 | 0.450 | 0.409 | 0.237 | 0.256 |
| $0.7 < \eta < 1.5$ | 0.750 | 0.617 | 0.593 | 0.428 | 0.327 | 0.146 | 0.173 | 0.174 |

which the track extrapolates and $|\mathcal{Q}_{\mathrm{muon}}| < 3.5$ (see Fig. 4).

### 2. Efficiency and misidentification rate measurements

The efficiency of the soft muon identification is measured using a pure sample of muons obtained from $J/\psi \rightarrow \mu\mu$ decays. These events are obtained using an online trigger requiring the presence of a muon with $p_T > 8$ GeV. The $J/\psi$ is reconstructed by requiring that the trigger muon make a vertex with another track of opposite charge that has associated muon chamber hits. All track requirements listed in Sec. V B 1 are applied to both tracks. The $J/\Psi$ candidate mass is required to satisfy $3.03 < m(\mu\mu) < 3.15$ GeV, and the sidebands of the mass distribution are used to evaluate the background under the mass peak.

The misidentification rates of pions and kaons are measured in $D^{*+} \rightarrow D^0 \pi^+$ decays, where the $D^0$ decays as $D^0 \rightarrow K^- \pi^+$. These events are obtained from a trigger that requires the presence of a vertex containing two tracks and are reconstructed requiring masses $1.835 < m(K\pi) < 1.895$ GeV and $m(D^*) - m(D^0) < 170$ MeV. The sidebands of the $m(D^*) - m(D^0)$ distribution are used to evaluate the background under the mass peak.

The misidentification rate of protons is measured using a sample of protons obtained from $\Lambda \rightarrow p\pi$ decays. These events are taken from the same data set as that from which the $D^*$ sample is obtained. The reconstructed $\Lambda$ mass is required to satisfy $1.111 < m(p\pi) < 1.121$ GeV. The sidebands of the mass distribution are used to evaluate the background under the mass peak.

Figure 4 (left panel) shows the distribution of muon scaled $\chi^2$, $\mathcal{Q}_{\mathrm{muon}}$, using the samples described above. Good separation is obtained between muons and other particle species.

An efficiency matrix is created in bins of $p_T$ and $\eta$ using the $J/\psi$ sample. Because the sample is limited in statistics for $p_T > 12$ GeV, empty bins are filled in using interpolation between the low-$p_T$ muons from $J/\Psi$ decays and higher-$p_T$ muons from $Z$ decays. The soft muon identification is applied to $Z$ events so that the region between the $J/\psi$ and $Z$ $p_T$ may be correctly fitted. Note that Fig. 4

shows the observed results in these low-statistics bins, while Table II shows the interpolated efficiencies.

For the corresponding binned misidentification matrix, the misidentification rate is measured in each of the three background samples. The $\pi$, $K$, and $p$ matrices are then combined in the proportion found in $W$ boson decays. These relative proportions are found to be $f(\pi) = 0.719$, $f(K) = 0.156$, and $f(p) = 0.125$.

The efficiency and fake rate as a function of $p_T$ is shown in Fig. 4. The efficiency in terms of $p_T$ and $\eta$ is tabulated in Table II. These identification rates are measured after the track and muon hit(s) have been identified.

This identification rate is applied as a weight to each candidate track in the MC to find the predicted number of identified electrons.

### 3. Soft muon systematic uncertainty determination

Separate systematic uncertainties are estimated for the true muon identification efficiency and the misidentification rate. The invariant mass sideband subtraction technique used to obtain the muon efficiency matrix introduces uncertainties arising from the statistics of the $J/\psi$ sample. These uncertainties vary from 2%–70%, depending on the bin in $p_T$ and $\eta$. In addition, the maximum variation in efficiency of 8% arising from the difference between isolated and nonisolated candidates is used as an uncertainty representing the maximum possible difference between the $J/\psi$ sample environment and the $W/Z$ environment. This is added in quadrature to the statistical uncertainty arising from the sideband subtraction method to obtain a final muon efficiency uncertainty of 8%–70%.

The misidentification systematic uncertainty is obtained by selecting muon-free regions in samples triggered on high-$p_T$ jets and taking the difference between observed and predicted soft muon misidentification rates. In this jet sample, at least three jets are required with $E_T > 15$ GeV and $|\eta| < 2.0$. In order to reduce the contamination from real muons, any jet that contains an identified heavy quark decay is rejected, as is any track that has impact parameter significance $d_0/\sigma(d_0) > 2$. In a sample having an online trigger requiring the presence of a jet with $E_T > 100$ GeV,

a difference of 4.8% is seen between the observed and predicted soft muon identification rates. A conservative estimate of twice this difference is used as the systematic uncertainty on the soft muon misidentification rate.

### C. Application of soft lepton identification to $W/Z$ samples

Additional selection criteria are applied to soft lepton candidates in the high $p_T$ $W$ and $Z$ boson data samples to reduce the amount of background in the search sample. Any track that is already identified as a high-$p_T$ electron or muon in the $W$ or $Z$ boson selection is ineligible to be identified as a soft muon. To reject badly measured tracks, each track is required to have at least one hit in the silicon detector. For electron candidates, this hit is required to be within the first two layers of the silicon detector to help reject photon conversions. Each track is required to be inside of a reconstructed jet having $|\eta| < 2.0$ and transverse energy of $E_T > 5$ GeV, so that the heavy flavor fraction fit described later in Sec. VI B can be applied. (Note that the "jet" could be composed entirely of leptons, or even entirely of a single lepton.) Any track that is identified as a conversion partner is rejected. The track candidate must have a distance along the beam line $|\Delta z| < 5$ cm from the high-$p_T$ trigger lepton. If the trigger lepton is the same flavor as the soft lepton, the invariant mass $M$ of the candidate and trigger is calculated, and the following mass ranges are rejected:

- $M < 5$ GeV to suppress the $J/\psi$ and $b\bar{b}$ backgrounds.
- $9 < M < 10$ GeV if the candidate track has opposite charge to the trigger lepton. This rejects $\Upsilon$ events.
- $80 < M < 100$ GeV if the candidate track has opposite charge to the trigger lepton. This rejects $Z$ events.

These additional selection criteria have a small effect on the benchmark model chosen for this analysis, cutting out 4.5% of the signal leptons generated.

### VI. BACKGROUND PREDICTION

The main SM backgrounds in this analysis are from $W$ + jets, Drell-Yan, QCD multijet, top quark, and diboson production processes. The cross section and differential distributions of electroweak backgrounds from hard scattering processes are modeled using the ALPGEN [29] MC program, except for the top production and diboson production backgrounds, which are modeled by PYTHIA [30]. PYTHIA is used to model the parton showering in all samples. These MC events are analyzed using a GEANT based detector simulation [31]. The samples generated by ALPGEN are $W/Z + N_p$ partons (light flavor) and $W + q\bar{q} + N_p$ partons, where $q = c$, $b$ (heavy flavor). The interface with the parton showering generates a double counting of heavy flavor events, which is corrected using the MLM matching method [32].

The relative contributions from the various background sources can be seen qualitatively in Fig. 2. The cross sections used for every sample are described in[24]. The final background predictions are summarized later in Sec. VII. The QCD multijet background requires a different treatment since it is not possible to simulate it using MC. It is derived using data as explained below.

### A. QCD multijet background fraction

The $W$ boson is identified by the presence of a high energy lepton and missing transverse energy. Events containing jets may emulate this signature; a dijet event, for example, may have large $\not{E}_T$ arising from the energy mismeasurement of one jet, while the other jet in the event can mimic an electron by leaving a track in the COT associated with an electromagnetic energy deposit. The contribution from these QCD multijet processes is estimated by using a data-derived model [33]. This is accomplished by defining an object that is similar to an electron, but has a much larger rate of contamination from jets; we refer to this as an "antiselected electron." An antiselected electron is required to pass the same kinematic requirements as an electron, but must fail at least two of the identification requirements.

The number of events arising from the QCD multijet background is obtained by fitting the $\not{E}_T$ distribution of the data using two templates: an electroweak template obtained from $W$ + jets, $Z$ + jets and diboson MC, and a QCD template. The QCD template is obtained from the antiselected electron sample after subtracting the expected $W$ boson contamination using the MC. The total number of events is kept constant and the fraction from each template is obtained from the fit.
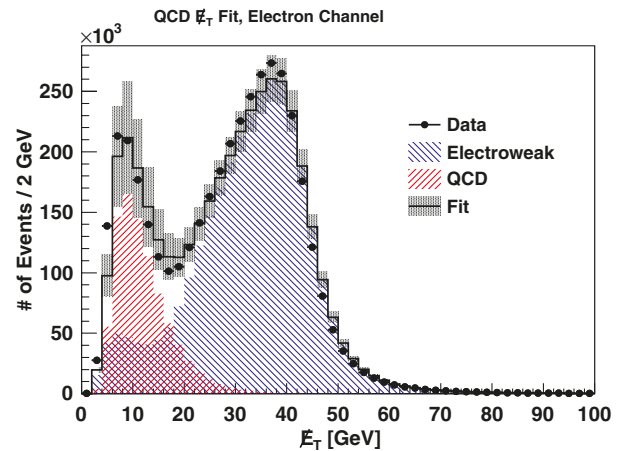


FIG. 5 (color online). The fit to the $\not{E}_T$ distribution of events with $m_T > 20$ GeV and $\Delta\phi(\not{E}_T, l) > 0.5$, in the electron-triggered data set. The "electroweak" template is obtained from Monte Carlo simulation, and the "QCD" template is obtained from the antiselected electron data sample. The systematic uncertainty of 26% found in [33] is shown.
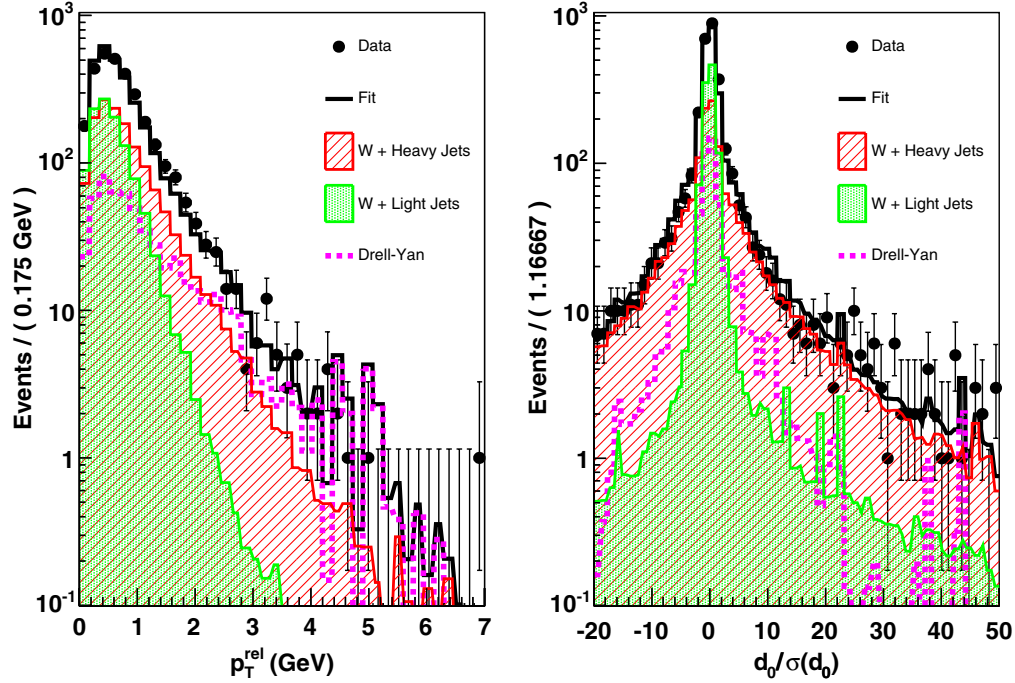
FIG. 6 (color online).    The result of the simultaneous fit of the $W + 1$ soft muon sample in the $p_T^{rel}$ and $d_0$ significance of the soft muon. The data distribution is fit to the sum of three components: $W$ + heavy quark, $W$ + light quark/gluon, and Drell-Yan.

After the fit is performed across the $\not{E}_T$ distribution, the number of QCD events in the $W$ boson signal region is calculated by applying the selection of $\not{E}_T > 25$ GeV. The MC electroweak contribution and the data-derived QCD template are scaled to the result obtained from this $\not{E}_T$ fit. Figure 5 shows the result of this fit in the electron-triggered data set. A similar fit is performed in each muon-triggered data set. A systematic uncertainty of 26% is applied to the QCD normalization, as found in [33].

### B. Heavy flavor background fraction

The leptonic decay of heavy flavor quarks creates a significant background contribution to the soft leptons of this analysis. This background is estimated using the data in the $W/Z$ plus exactly one soft muon channel, which should be dominated by SM processes. A fit is performed in two distributions of soft muons which are sensitive to the heavy flavor fraction: $p_T^{rel}$, which is the momentum of the muon transverse to the direction of the jet in which it is found, and $d_0/\sigma(d_0)$, which is the significance of the muon's impact parameter with respect to the beam line. A simultaneous fit is performed of these two distributions to a sum of templates from heavy flavor, light flavor, and Drell-Yan processes, as shown in Fig. 6. These templates were acquired from the MC background samples. The result of this fit is used to normalize the contributions of the three types of processes in the higher-multiplicity sample. The uncertainty resulting from the fit, ranging from 5% to 34% in the various samples, is used as a systematic uncertainty on this normalization.

### C. Normalization of soft electron multiplicities

The heavy flavor fit described in Sec. VI B normalizes all of the data to the $W/Z + 1\mu$ channel. However, we find a mismatch in the $W/Z + 1e$ channel, which has a large contribution from photon conversions. The difference between the predicted and observed numbers in the $W/Z$ plus exactly one electron channel is 34% in the $W$ boson sample and 31% in the $Z$ boson sample. This is used as a systematic uncertainty for the normalization of all other MC with at least one additional identified electron [24].

### VII. RESULTS

Using the soft lepton identification techniques described in Sec. V, we count the numbers of $W$ and $Z$ boson events with multiple additional leptons. Figures 7 and 8 show the multiplicity of additional electrons ($N_e$) and muons ($N_\mu$) in these events, with the SM expectation and observed data overlaid. The two-dimensional histograms of $N_\mu$ vs $N_e$ are presented in slices of $N_e$ for ease of viewing. These expected and observed event counts are also presented in Tables III and IV for ease of comparison with predictions from other models. The sources of systematic uncertainties are summarized in Table V, with references to the sections in which they are described and evaluated. Good agreement with the SM expectation is observed across the distributions.

In particular, very few multimuon events are observed. This is the region where many lepton jet models would be expected to show an excess, since a potential signal in the
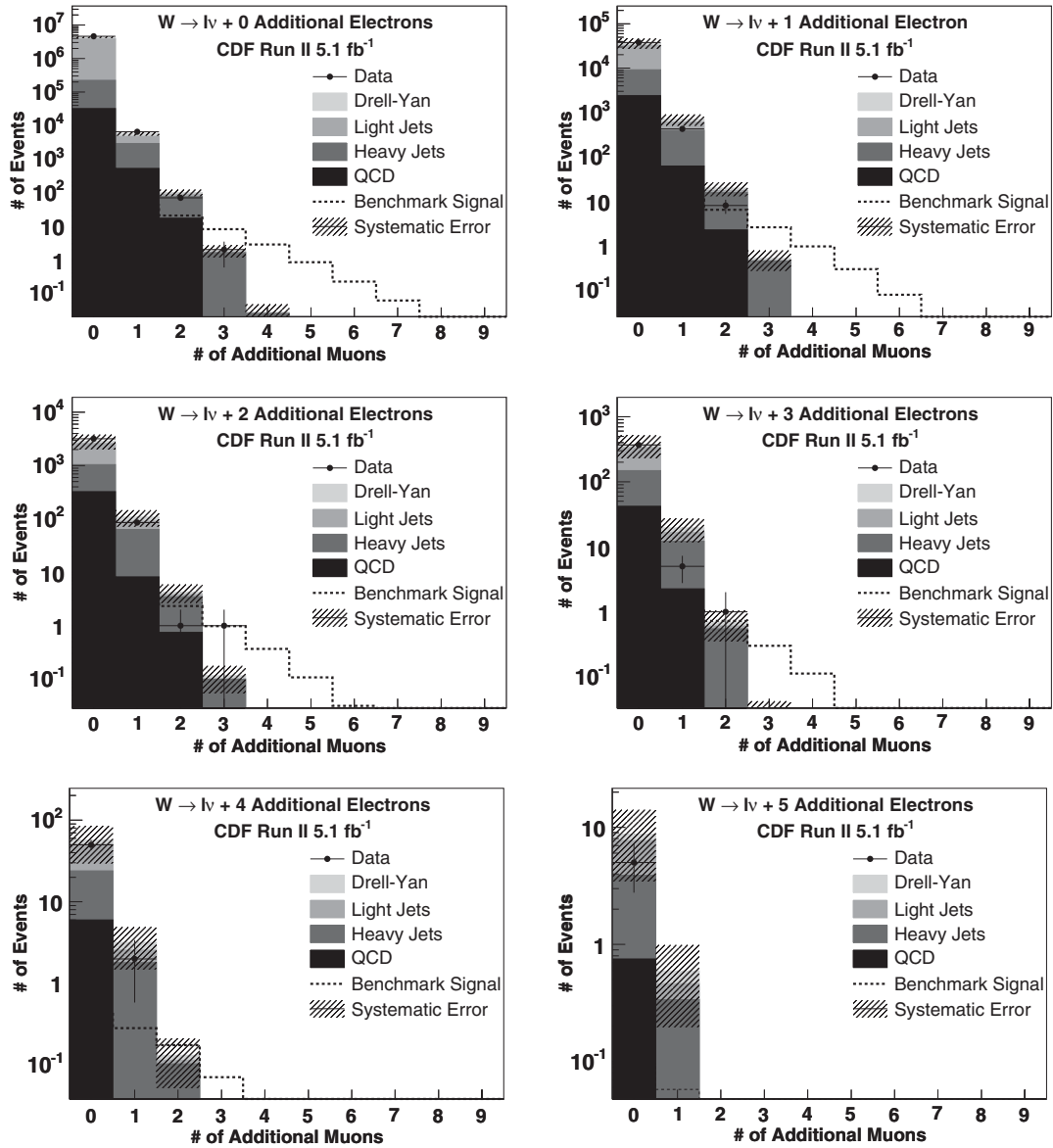
FIG. 7.   Multiplicity of additional electrons and muons after the $W$ boson selection. The two-dimensional histogram of $N_\mu$ vs $N_e$ is presented in slices of $N_e$ for ease of viewing. Both hard and soft leptons (but not the initial lepton used for the $W$ boson selection) are counted. Note that the distributions combine the electron- and muon-triggered events.

multielectron region would be more likely to be hidden by the large background contribution from photon conversions. Only three events containing three muons beyond the $W$ selection are observed, which is consistent with the SM expectation of 2.9 events. No events are observed containing four or more additional muons.

## A. Benchmark model

This is a general signature-based search, and as such is applicable to many different models. We choose an example model from the representative lepton jet models presented in Ref. [8]. The benchmark model chosen for this analysis is an adaptation of the "neutralino benchmark model," in which the Higgs decays principally to a pair of

the lightest supersymmetric particles, which then decay through a dark sector to lepton jets. A MC sample of signal events was generated from this model using PYTHIA. The signal from this model to which this analysis is most sensitive is the associated production of a $W$ or $Z$ boson and a Higgs boson, which has a cross section of 389 fb. This cross section would result in 1647 $W$ + Higgs events and 322 $Z$ + Higgs events in the data sample of this analysis before applying any selection criteria.

The particular parameters of the model [34] were chosen to create a "typical" model of this class. The MSSM parameters [$\mu$, $m_1$, $m_2$, $\tan(\beta)$, and $\sin(\alpha)$] avoid previous limits from searches for supersymmetry while making the lightest supersymmetric partner ($\chi_0$) the favored Higgs

TABLE III. Summary of predicted and observed event counts by number of additional electrons ($N_e$) and muons ($N_\mu$) after the $W$ boson selection. The prediction of a model described in Sec. VII A is also shown for comparison. Bins with less than 0.25 expected events in both signal and background and 0 observed events are not shown.

| $N_e$ | $N_\mu$ | Predicted SM background | Predicted dark Higgs signal | Observed |
|---|---|---|---|---|
| 0 | 0 | $4\,623\,512 \pm 315\,244$ | 158 | 4 673 896 |
| 0 | 1 | $6463 \pm 807$ | 42 | 6498 |
| 0 | 2 | $109 \pm 24$ | 21 | 70 |
| 0 | 3 | $2.1 \pm 0.79$ | 8.0 | 2 |
| 0 | 4 | $0.029 \pm 0.019$ | 2.8 | 0 |
| 0 | 5 | $0.000\,26 \pm 0.000\,23$ | 0.83 | 0 |
| 1 | 0 | $46\,055 \pm 11\,387$ | 27 | 37 778 |
| 1 | 1 | $824 \pm 230$ | 11 | 425 |
| 1 | 2 | $23 \pm 7.8$ | 6.4 | 8 |
| 1 | 3 | $0.58 \pm 0.27$ | 2.6 | 0 |
| 1 | 4 | $0.010 \pm 0.0074$ | 0.95 | 0 |
| 1 | 5 | $0.000\,11 \pm 0.000\,11$ | 0.29 | 0 |
| 2 | 0 | $3600 \pm 1085$ | 7.1 | 3184 |
| 2 | 1 | $129 \pm 43$ | 3.8 | 86 |
| 2 | 2 | $4.9 \pm 1.8$ | 2.3 | 1 |
| 2 | 3 | $0.13 \pm 0.067$ | 0.97 | 1 |
| 2 | 4 | $0.0031 \pm 0.0024$ | 0.37 | 0 |
| 3 | 0 | $491 \pm 185$ | 1.9 | 366 |
| 3 | 1 | $23 \pm 9.3$ | 1.2 | 5 |
| 3 | 2 | $0.85 \pm 0.42$ | 0.72 | 1 |
| 3 | 3 | $0.028 \pm 0.017$ | 0.30 | 0 |
| 4 | 0 | $79 \pm 38$ | 0.47 | 50 |
| 4 | 1 | $3.9 \pm 2.1$ | 0.28 | 2 |
| 5 | 0 | $13 \pm 7.6$ | 0.096 | 5 |
| 5 | 1 | $0.74 \pm 0.49$ | 0.058 | 0 |
| 6 | 0 | $2.0 \pm 1.5$ | 0.015 | 0 |

TABLE IV. Summary of predicted and observed event counts by number of additional electrons ($N_e$) and muons ($N_\mu$) after the $Z$ selection. The prediction of a model described in Sec. VII A is also shown for comparison. Bins with less than 0.25 expected events in both signal and background and 0 observed events are not shown.

| $N_e$ | $N_\mu$ | Predicted SM background | Predicted dark Higgs signal | Observed |
|---|---|---|---|---|
| 0 | 0 | $215\,219 \pm 36\,886$ | 7.6 | 211 448 |
| 0 | 1 | $255 \pm 52$ | 1.2 | 270 |
| 0 | 2 | $3.2 \pm 0.89$ | 0.54 | 4 |
| 1 | 0 | $2145 \pm 447$ | 1.0 | 1975 |
| 1 | 1 | $30 \pm 8.1$ | 0.27 | 20 |
| 1 | 2 | $0.51 \pm 0.18$ | 0.15 | 0 |
| 2 | 0 | $175 \pm 50$ | 0.28 | 176 |
| 2 | 1 | $4.2 \pm 1.5$ | 0.10 | 5 |
| 3 | 0 | $23 \pm 9.0$ | 0.070 | 18 |
| 3 | 1 | $0.71 \pm 0.31$ | 0.031 | 1 |
| 4 | 0 | $3.4 \pm 1.8$ | 0.019 | 2 |
| 5 | 0 | $0.52 \pm 0.35$ | 0.0044 | 0 |

TABLE V. Sources of systematic uncertainties. Their size is measured both as a percentage and as the number of events in a benchmark-signal-rich region, defined as a $W$ or $Z$ boson plus at least three additional muons with $p_T > 3$ GeV. Note that, although some of the systematics are large, they have little effect in the signal region due to there being negligible SM background.

| Systematic source | Size | Effect in large S/B region (events) |
|---|---|---|
| Trigger efficiency [24] | $\pm(1.6–5.9)\%$ | $\pm 0.06$ |
| QCD fraction (Sec. VI A) | $\pm 26\%$ | 0 |
| Soft $e$ real rate (Sec. V A 3) | $\pm 15\%$ | $\pm 0.04$ |
| Soft $e$ fake rate (Sec. V A 3) | $\pm 15\%$ | $\pm 0.11$ |
| Soft $\mu$ real rate (Sec. V B 3) | $\pm(8–70)\%$ | $\pm 0.64$ |
| Soft $\mu$ fake rate (Sec. V B 3) | $\pm 10\%$ | $\pm 0.34$ |
| Soft $e$ normalization (Sec. VI C) | $\pm(31–39)\%$ | $\pm 0.24$ |
| Heavy flavor fraction (Sec. VI B) | $\pm(5–34)\%$ | $\pm 0.25$ |

decay channel. The Higgs has a mass near that favored by precision measurements. The branching fractions for $\chi_0$ decaying into the dark neutralinos ($\chi_d$) and dark photons ($\gamma_d$) simply model the sort of cascade decay illustrated in Fig. 1. The mass of the dark photon is chosen in order to make the additional leptons that are produced approximately half muons and half electrons. These parameters are summarized in Table VI.

We set a 95% confidence level limit on the production of this benchmark model. The limit is set at $0.312 \times \sigma$, or 112 fb. The model can be ruled out at the standard cross section at a confidence level of 99.7%. Both of these limits are set in the Bayesian framework using the MCLIMIT tools [35] running over the combined $W$ and $Z$ channels in Figs. 7 and 8 (Tables III and IV).

TABLE VI. Parameters used for the benchmark model based on that in Ref. [8]. The first five parameters are the inputs to the MSSM including the branching fractions for $\chi_0 \to \chi_d + N\gamma_d$ [34].

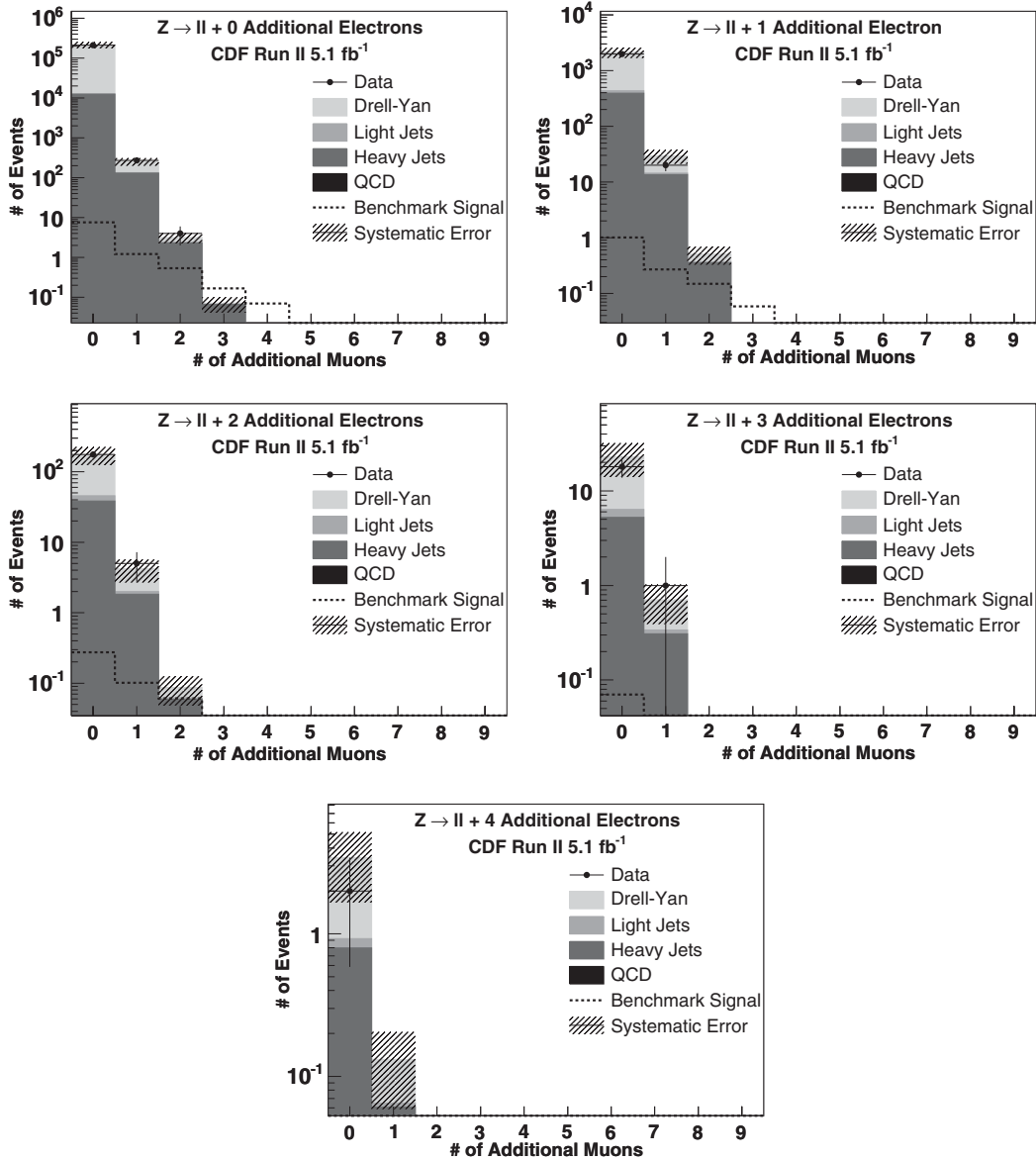| Parameter | Value |
|---|---|
| $\mu$ | 149 GeV |
| $m_1$(bino) | 13 GeV |
| $m_2$(wino) | 286 GeV |
| $\tan(\beta)$ | 3.5 |
| $\sin(\alpha)$ | $-0.28$ |
| $m_{\chi_0}$ | 10 GeV |
| $m_H$ | 120 GeV |
| $m_{\chi_d}$ | 1 GeV |
| $m_{\gamma_d}$ | 300 MeV |
| BR($\chi_0 \to \chi_d + 2\gamma_d$) | 33% |
| BR($\chi_0 \to \chi_d + 3\gamma_d$) | 33% |
| BR($\chi_0 \to \chi_d + 4\gamma_d$) | 33% |

FIG. 8.  Multiplicity of additional electrons and muons after the $Z$ selection. The two-dimensional histogram of $N_\mu$ vs $N_e$ is presented in slices of $N_e$ for ease of viewing. Both hard and soft leptons (but not the initial leptons used for the $Z$ boson selection) are counted. Note that the distributions combine the electron- and muon-triggered events.

## B. Application to other models

In addition to the benchmark model discussed in Sec. VII A, limits can be set on a wide range of alternate models. A rough estimate of the limit for a particular model can be made by normalizing its production to the $W$ or $Z$ boson cross section, applying the efficiencies in Tables I and II to the additional leptons, and comparing the result to the observed and predicted numbers of additional leptons in Tables III and IV. For ease of reference, a summary of the kinematic selections for identified objects is presented in Table VII.

In general, any model that predicts significant numbers of three-muon events can be ruled out, since only three such events are observed in the sample, consistent with the

SM background. However, models that produce multiple electrons can more easily be accommodated, since photon conversions result in a much higher background in that region.

## VIII. CONCLUSIONS

This analysis expands the reach of previous searches for additional leptons by allowing leptons to be reconstructed from a much lower $p_T$ threshold and with no requirement of isolation. This greatly increases the acceptance to find lepton jets or similar excesses of leptons from effects beyond the SM. No indication of such new effects is seen in the data sample. A 95% confidence level limit is set on an example benchmark model of supersymmetric Higgs

TABLE VII. Summary of kinematic requirements to find various objects. These numbers can be used to set limits on many models that predict the production of additional leptons.

| Object | Requirements | Number observed |
|---|---|---|
| $W$ | $p_T(e/\mu) > 20$ GeV<br>$|\eta(e)| < 1.1$, $|\eta(\mu)| < 1.5$<br>$\not{E}_T > 25$ GeV<br>$m_T(l, \not{E}_T) > 20$ GeV<br>$d\phi(l, \not{E}_T) > 0.5$ | 4 722 370 |
| $Z$ | $p_T(e/\mu) > 20$ GeV<br>$p_T(e_2) > 12$ GeV, $p_T(\mu_2) > 10$ GeV<br>$|\eta(e)| < 1.1$, $|\eta(\mu)| < 1.5$<br>76 GeV $< m(l_1, l_2) < 106$ GeV | 342 291 |
| Soft $e$ | $p_T(e) > 2$ GeV<br>$|\eta(e)| < 1$<br>$\mathcal{L} > 0.99$ (Efficiency in Table I) | See Tables III and IV |
| Soft $\mu$ | $p_T(\mu) > 3$ GeV<br>$|\eta(\mu)| < 1.5$<br>$|\mathcal{L}| < 3.5$ (Efficiency in Table II) | See Tables III and IV |

production, and a framework is provided to set limits on a class of other models.

[1] R. Dermisek and J. F. Gunion, Phys. Rev. Lett. **95**, 041801 (2005); Phys. Rev. D **75**, 075019 (2007).

[2] C. T. Hill and R. J. Hill, Phys. Rev. D **75**, 115009 (2007); **76**, 115014 (2007).

[3] C. Cheung, J. T. Ruderman, L. Wang, and I. Yavin, J. High Energy Phys. 04 (2010) 116.

[4] N. Arkani-Hamed, D. P. Finkbeiner, T. R. Slayter, and N. Weiner, Phys. Rev. D **79**, 015014 (2009); P. Meade, M. Papucci, A. Strumia, and T. Volansky, Nucl. Phys. **B831**, 178 (2010); M. Pospelov and A. Ritz, Phys. Lett. B **671**, 391 (2009); C. Cheung, J. T. Ruderman, L. T. Wang, and I. Yavin, Phys. Rev. D **80**, 035008 (2009); A. Katz and R. Sundrum, J. High Energy Phys. 06 (2009) 003.

[5] J. T. Ruderman and T. Volansky, J. High Energy Phys. 02 (2010) 024; X. Chen, J. Cosmol. Astropart. Phys. 09 (2009) 029; J. Mardon, Y. Nomura, and J. Thaler, Phys. Rev. D **80**, 035013 (2009).

[6] T. Aaltonen et al. (CDF Collaboration), Phys. Rev. D **83**, 112008 (2011).

[7] T. Aaltonen et al. (CDF Collaboration), Phys. Rev. Lett. **101**, 251801 (2008); V. M. Abazov et al. (D0 Collaboration), Phys. Lett. B **680**, 34 (2009); CMS Collaboration, Phys. Lett. B **704**, 411 (2011); ATLAS Collaboration, Eur. Phys. J. C **71**, 1647 (2011).

[8] A. Falkowski, J. T. Ruderman, T. Volansky, and J. Zupan, J. High Energy Phys. 05 (2010) 077; Phys. Rev. Lett. **105**, 241801 (2010).

[9] V. M. Abazov et al. (D0 Collaboration), Phys. Rev. Lett. **105**, 211802 (2010).

[10] CMS Collaboration, J. High Energy Phys. 07 (2011) 098.

[11] We use the convention that "momentum" refers to $pc$ and "mass" to $mc^2$.

[12] The CDF-II detector uses a cylindrical coordinate system in which $\phi$ is the azimuthal angle, $r$ is the radius from the nominal beam line, and $z$ points in the proton beam

direction. The transverse ($r$-$\phi$) plane is perpendicular to the $z$ axis. Transverse momentum and energy are the respective projections of momentum measured in the tracking system and energy measured in the calorimeter system onto the $r$-$\phi$ plane, and are defined as $p_T = p \sin\theta$ and $E_T = E \sin\theta$. Here, $\theta$ is the polar angle measured with respect to the interaction vertex. Missing $E_T$ ($\vec{\not{E}}_T$) is defined by $\vec{\not{E}}_T = -\sum_i E_T^i \hat{n}_i$, where $i$ is the calorimeter tower number for $|\eta| < 3.6$, and $\hat{n}_i$ is a unit vector perpendicular to the beam axis and pointing at the $i$th tower. The transverse mass $m_T$ is defined as the invariant mass of the sum of the transverse projection of the momentum vector of one decay product and the missing energy vector $\vec{\not{E}}_T$. The pseudorapidity $\eta$ is defined as $-\ln(\tan(\theta/2))$, where $\theta$ is measured with respect to the origin of the detector. We define the magnitude $\not{E}_T = |\vec{\not{E}}_T|$.

[13] A. Abulencia *et al.*, J. Phys. G **34**, 2457 (2007).

[14] F. Abe *et al.*, Nucl. Instrum. Methods Phys. Res., Sect. A **271**, 387 (1988); D. Acosta *et al.* (CDF Collaboration), Phys. Rev. D **71**, 052003 (2005); The CDF-II Detector Technical Design Report No. Fermilab-Pub-96/390-E; A. Abulencia *et al.* (CDF Collaboration), J. Phys. G **34**, 2457 (2007); T. Aaltonen *et al.* (CDF Collaboration), Phys. Rev. D **77**, 112001 (2008).

[15] A. Sill *et al.*, Nucl. Instrum. Methods Phys. Res., Sect. A **447**, 1 (2000); A. Affolder *et al.*, Nucl. Instrum. Phys. Res., Sect. A **453**, 84 (2000); C. S. Hill *et al.*, Nucl. Instrum. Methods Phys. Res., Sect. A **530**, 1 (2004).

[16] A. Affolder *et al.*, Nucl. Instrum. Methods Phys. Res., Sect. A **526**, 249 (2004).

[17] L. Balka *et al.*, Nucl. Instrum. Methods Phys. Res., Sect. A **267**, 272 (1988).

[18] S. Bertolucci *et al.* Nucl. Instrum. Methods Phys. Res., Sect. A **267**, 301 (1988).

[19] S. Kuhlmann, H. Frisch, M. Cordelli, J. Huston, R. Miller, S. Lami, R. Paoletti, N. Turini, M. Iori, D. Toback, and F.

[20] G. Ascoli, L. E. Holloway, I. Karliner, U. E. Kruse, R. D. Sard, V. J. Simaitis, D. A. Smith, and T. K. Westhusing, Nucl. Instrum. Methods Phys. Res., Sect. A **268**, 33 (1988); A. Artikov *et al.*, Nucl. Instrum. Methods Phys. Res., Sect. A **538**, 358 (2005).

[21] D. Acosta *et al.* (CDF Collaboration), Nucl. Instrum. Methods Phys. Res., Sect. A **461**, 540 (2001); D. Acosta, S. Klimenko, J. Konigsberg, A. Korytov, G. Mitselmakher, V. Necula, A. Nomerotsky, A. Pronko, A. Sukhanov, A. Safonov, D. Tsybychev, S. M. Wang, and M. Wong, Nucl. Instrum. Methods Phys. Res., Sect. A **494**, 57 (2002).

[22] D. Acosta *et al.* (CDF Collaboration), Phys. Rev. Lett. **94**, 091803 (2005).

[23] F. Abe *et al.* (CDF Collaboration), Nucl. Instrum. Methods Phys. Res., Sect. A **271**, 387 (1988).

[24] S. Wilbur, Ph.D. thesis, University of Chicago, 2011.

[25] S. Paramonov, Ph.D. thesis, University of Chicago, 2009.

[26] T. Aaltonen *et al.* (CDF Collaboration), Phys. Rev. D **82**, 112005 (2010).

[27] A. Abulencia *et al.* (CDF Collaboration), J. Phys. G **34**, 2457 (2007).

[28] D. Acosta *et al.* (CDF Collaboration), Phys. Rev. D **72**, 032002 (2005).

[29] M. L. Mangano, M. Moretti, F. Piccinini, R. Pittau, and A. Polosa, J. High Energy Phys. 07 (2003) 001.

[30] T. Sjostrand, S. Mrenna, and P. Skands, J. High Energy Phys. 05 (2006) 026.

[31] E. Gerchtein and M. Paulini, arXiv:0306.031.

[32] S. Hoeche *et al.*, arXiv:0602.031.

[33] B. Cooper, Ph.D. thesis, University College London [Report No. FERMILAB-THESIS-2006-61, 2006].

[34] M. Reece (private communication).

[35] T. Junk, Nucl. Instrum. Methods Phys. Res., Sect. A **434**, 435 (1999).